

Photopolarimetric observations of the new eclipsing polar CTCV J1928-5001.

Stephen B. Potter¹, Thomas Augusteijn² & Claus Tappert³

¹*South African Astronomical Observatory, PO Box 9, Observatory 7935, Cape Town, South Africa*

²*Nordic Optical Telescope, Apartado 474, 38700 Santa Cruz de La Palma, Canary Islands, Spain*

³*Departamento de Astronomía y Astrofísica, Pontificia Universidad Católica, Casilla 306, Santiago 22, Chile*

ABSTRACT

We report photopolarimetric observations of a new eclipsing polar (AM Herculis system) discovered in the Calán-Tololo survey. The photometry and polarimetry are modulated on a period of ~ 101 minutes. Circular polarization variations are seen from ~ -8 to $+12$ per cent and from ~ 0 to 5 per cent in the red and blue parts of the optical spectrum, respectively. Two linearly polarized pulses are detected at orbital phases coinciding with the reversals in the circular polarization. This is consistent with a magnetic field strength of ~ 20 MG for the white dwarf primary, where accretion takes place at two regions. Both accretion regions are self-occulted by the white dwarf during parts of the orbit. We estimate some of the system's parameters from its eclipses, which we further refine by modelling the polarimetric observations.

Key words: accretion, accretion discs – methods: analytical – techniques: polarimetric – binaries: close – novae, cataclysmic variables – X-rays: stars.

1 INTRODUCTION

Polars (AM Herculis systems) are short period binaries that contain a white dwarf (known as the primary star) and a red dwarf (the secondary star) that overflows its Roche lobe. The magnetic field of the white dwarf is sufficiently strong to lock the system into synchronous rotation and to prevent an accretion disc from forming. Instead, the overflowing material from the secondary star initially continues on a ballistic trajectory until, at some distance from the white dwarf, the magnetic pressure overwhelms the ram pressure of the ballistic stream. From this point onwards the accretion flow is confined to follow the magnetic field lines of the white dwarf, see e.g. Cropper (1990) or Warner (1995) for a full review of magnetic cataclysmic variables (mCVs).

In high inclination systems, the secondary star occults the white dwarf, the accretion region and the magnetic and ballistic accretion streams, which produces structured photometric eclipse profiles. Thus eclipses offer unique opportunities to investigate these spatial structures and to constrain the binary parameters (e.g. HU Aqr: Hakala et al. 1993 and Bridge et al. 2002, UZ For: Imamura, Steiman-Cameron & Thomas 1998 and V1309: Katajainen et al. 2003). In addition, the polarimetric variations can give further insights into the accretion region. With appropriate modelling, one can estimate the shape, size and location of the accretion region on the surface of the white dwarf (e.g. Bailey et

al. 1995 and Potter, Hakala & Cropper 1998), which aids the determination of the magnetic field structure of the white dwarf and the extent of the ballistic and magnetic streams. Knowing the location of the accretion region also helps to interpret spectroscopic observations: the cyclotron and bremsstrahlung radiation emitted from the accretion region is reprocessed by the other binary components and is seen as, for example, modulated emission line variations (see e.g. Schwöpe et al. 2000, Romero-Colmenero et al. 2003).

CTCV J1928-5001 was identified spectroscopically and photometrically in the Calán-Tololo survey (see Tappert, Augusteijn & Maza 2004) as an AM Her system candidate. In this paper, our follow-up high time-resolved photometry has confirmed its CV characteristics with an orbital modulation of ~ 101 minutes interspersed by deep, short eclipses. The optical light-curve is characterised by a double-humped bright phase and a faint phase. The eclipse ingresses and egresses are particularly sharp, typically 2-3 seconds in duration, which have enabled us to calculate an accurate eclipse ephemeris. The eclipse itself is relatively short in duration, lasting ~ 177 seconds. We discuss the shape of the eclipse profile and the constraints that it places on the binary parameters, such as its inclination, mass-ratio and white dwarf mass.

In addition, we use Stokes imaging (see Potter, Hakala & Cropper 1998 and Potter et al. 2004) to model the polarimetric observations and we show that accretion takes place

at two regions on the primary. We place further constraints on the binary parameters by combining the analysis of the eclipses and the polarimetric modelling with simple single particle trajectory modelling.

2 OBSERVATIONS

2.1 Photometry

The 2003 photometric observations were obtained as part of the polarimetric observations. Over the course of three nights, unfiltered (defined by an RCA31034A GaAs photomultiplier response 3500 – 9000 Å), OG570 filtered and BG39 filtered light curves were acquired. Conditions were photometric during the whole observing campaign. The data were sky subtracted and extinction corrected, but not flux calibrated. From the observed count rate, however, we estimate that the system was caught in a brighter state (V magnitude ~ 16 -17) than the 1996 observations (Tappert, Augusteijn & Maza 2004). Figs. 1, 2, 3 & 4 show the eclipse profiles and the folded light curves respectively.

2.2 Polarimetry

CTCV J1928-5001 was observed on three nights during August 2003 (see table 1) using the South African Astronomical Observatory (SAAO) 1.9-m telescope and the UCT polarimeter (UCTPol; Cropper 1985). The UCTPol was operated in Stokes mode, i.e. simultaneous linear and circular polarimetry, and photometry. Broad filtered (BG39 and OG570 covering 3500 – 5500 Å and 5700 – 9000 Å respectively) and white light (defined by an RCA31034A GaAs photomultiplier response 3500 – 9000 Å), observations were taken (see Figs. 2, 3 & 4).

Polarised standard stars (Hsu & Breger 1982) were observed during the nights to set the position angle offsets. Non-polarized standard stars and calibration polaroids were observed to set the efficiency factors. Background sky polarisation measurements were also taken at frequent intervals during the observations. Polynomial fits to the sky measurements were subtracted from the object measurements. The data were reduced as described in Cropper (1997).

3 ANALYSIS

3.1 The eclipses

Fig. 1 shows the ten eclipses observed in 2003. Upon inspection of the 2003 eclipses, we identify seven features which vary from one eclipse to another and may be wavelength-dependent. These features are indicated in Fig. 1d, where they appear most pronounced. They are also listed below in order of increasing time, and we interpret them using geometric arguments based on the standard picture of an mCV.

1. There is first a slow decrease in brightness of length $\sim 15 - 20$ s. We attribute this to the gradual ingress of the stream beginning at the inner Lagrangian point.

2. Next, there is a plateau of almost constant brightness for $\sim 40 - 45$ s. With the stream now mostly eclipsed, the plateau can be interpreted as emission from the photosphere of the white dwarf and from the accretion region.

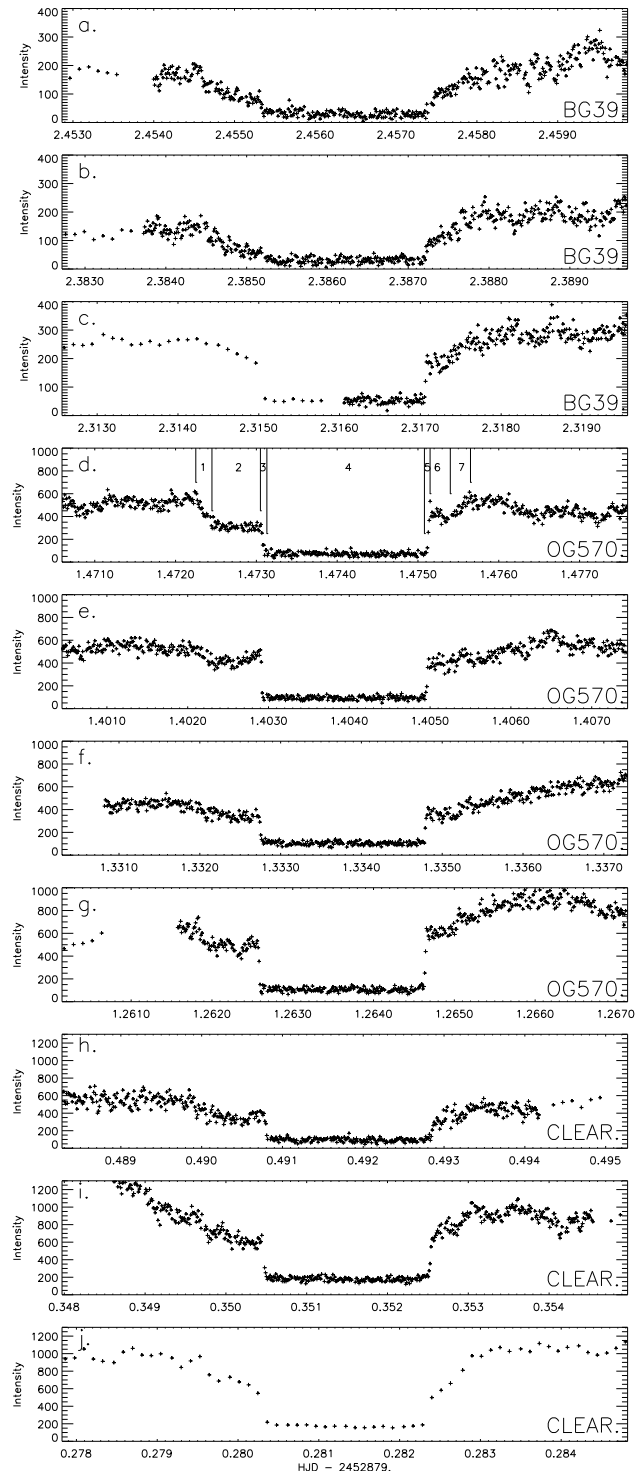


Figure 1. The eclipses centered on the orbital period. a,b and c are taken through a BG39 filter, d,e,f and g are taken through an OG570 filter and h,i and j are unfiltered.

Table 1. Log of observations. ‘1.9m SAAO’ is the 1.9m telescope of the South African Astronomical Observatory. ‘UCTPol’ is the University of Cape Town photopolarimeter. ‘Eclipses’ indicates the number of eclipses each observation covered. ‘10 + 1s’ means that we obtained 10 and 1 second time resolution out and during eclipse, respectively.

date	telescope	instrument	filter	time resolution	eclipses
27 Aug 2003	1.9m SAAO	UCTPol	Unfiltered	10 + 1 s	3
28 Aug 2003	1.9m SAAO	UCTPol	OG570	10 + 1 s	4
29 Aug 2003	1.9m SAAO	UCTPol	BG39	10 + 1 s	3

Table 2. Table of eclipse timings. Ingress, egress and mid-eclipses are HJD-2450000. The 1996 eclipses were recalculated from the observations of Tappert, Augusteijn & Maza 2004 (see text).

Date	Ingress	Egress	Mid-eclipse	Cycle
8 Jul 1996	273.7286(32)	273.7382(32)	273.7334(55)	-37136
8 Jul 1996	273.8016(13)	273.8056(13)	273.8036(23)	-37135
9 Jul 1996	274.7135(11)	274.7179(11)	274.7157(19)	-37122
9 Jul 1996	274.7846(11)	274.7878(11)	274.7862(19)	-37121
9 Jul 1996	274.8538(11)	274.8592(11)	274.8565(19)	-37120
30 Jul 1996	295.62312(69)	295.6259(7)	295.6245(12)	-36824
30 Jul 1996	295.69125(69)	295.6973(7)	295.6947(12)	-36823
27 Aug 2003	2879.28030(12)	2879.28234(12)	2879.28132(16)	0
27 Aug 2003	2879.350472(12)	2879.352527(12)	2879.351500(16)	1
27 Aug 2003	2879.490793(12)	2879.492859(12)	2879.491826(16)	3
28 Aug 2003	2880.262589(12)	2880.264638(12)	2880.263614(16)	14
28 Aug 2003	2880.332752(12)	2880.334801(12)	2880.333777(16)	15
28 Aug 2003	2880.402916(12)	2880.404953(12)	2880.403934(16)	16
28 Aug 2003	2880.473073(12)	2880.475116(12)	2880.474095(16)	17
29 Aug 2003	2881.31496(12)	2881.317063(12)	2881.31601(12)	29
29 Aug 2003	2881.385212(12)	2881.387214(12)	2881.386213(16)	30
29 Aug 2003	2881.455323(12)	2881.457407(12)	2881.456366(16)	31

This is further supported by the continued presence of circular polarization during this period (not shown). In some cases (e.g. Fig. 1 a,b and i) the plateau is not so obvious; this may indicate that the extent and/or brightness of the stream changes over time.

3. There is next a rapid drop in brightness to $\sim 20\%$ of maximum intensity which takes only ~ 3 seconds. The phase of the rapid drop appears to be very stable between the observed eclipses (see Fig. 1) and the magnitude of the dip appears to be wavelength-dependent. Therefore, we attribute this feature to the ingress of the white dwarf and the accretion region. The data is of insufficient time resolution and/or signal-to-noise to resolve the eclipse of the photosphere of the white dwarf and the accretion region separately. (see e.g. the eclipse of UZ For: Imamura, Steiman-Cameron & Thomas 1998).

In general, the trajectory of the stream is expected to result in the stream lagging the white dwarf and, consequently, eclipsing later than the white dwarf and the accretion region. Therefore, we would expect to see the phase of slower decline in brightness to follow the rapid drop (e.g. HU Aqr: Hakala et al. 1993 and Bridge et al. 2002, UZ For: Imamura, Steiman-Cameron & Thomas 1998 and V1309: Katajainen

et al. 2003). Since this phase is before the rapid drop, we reason that, in this system, the brightest part of the stream is mostly eclipsed by now, and there is little or insignificant emission from the latter parts of the accretion stream.

4. Next, the light curve takes on a flat minimum, which can be associated with the complete eclipse of the white dwarf and the accretion stream. This feature lasts just under three minutes.

5. The total eclipse is terminated by a rapid increase in intensity ($\sim 500\%$) in $\sim 3-4$ seconds. We attribute this to the egress of the white dwarf and the accretion region. Again, as with the ingresses, the egresses appear to be stable in phase between eclipses. These data are also of insufficient time resolution and/or signal-to-noise to resolve the photosphere of the white dwarf and the accretion region separately.

6. Next follows a short plateau of constant brightness lasting $\sim 15 - 20s$. This is most likely due to emission from the photosphere of the white dwarf and the accretion region. This is again further supported by the presence of circular polarization during this period (not shown). As with the plateau before ingress (note 2 above), the length of this post-eclipse plateau is not so obvious in some cases. This again

Table 3. Table of system parameters. The mass of the secondary is assumed to be $0.1M_{\odot}$ and the eclipse length to be $\Delta\phi = 0.029$. β is the angle between the magnetic axis and the spin axis of the white dwarf. The range in the white dwarf radius is estimated from In-Saeng Suh & Mathews (2000)

Inclination (degrees)	β (degrees)	mass ratio (M_2/M_1)	White dwarf mass/ M_{\odot}	White dwarf radius $\times 100/R_{\odot}$
70	29	0.97	0.10	1.7 - 2.3
74	23	0.42	0.24	1.3 - 1.7
78	18	0.20	0.50	1.0 - 1.3
82	12	0.07	1.43	< 1.0

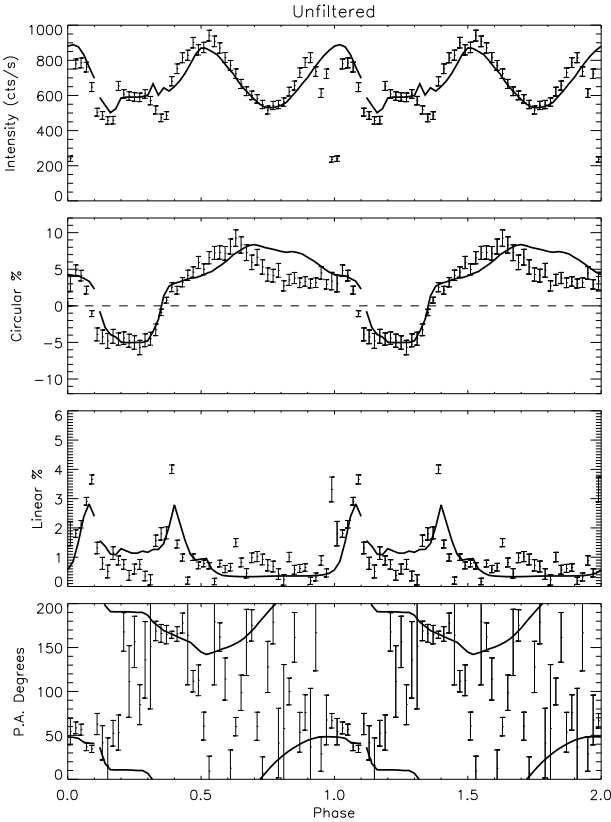


Figure 2. The polarimetric data (white light) folded on the eclipse ephemeris derived in section 3.2. Solid curves are the model fit (see section 3.6)

may indicate that the extent and/or brightness of the stream changes over time.

7. Finally, the intensity slowly increases to the pre-eclipse level, as the brighter parts of the accretion stream gradually come into view.

3.2 An eclipse ephemeris

We re-analyzed the observations of Tappert, Augustejn & Maza (2004) and discovered that, due to a software error, part of their dataset had not been heliocentric corrected, leading to an erroneous ephemeris. We therefore recalculated the times of the ingresses and egresses of the 1996 observations. Since the 1996 eclipses contained unre-

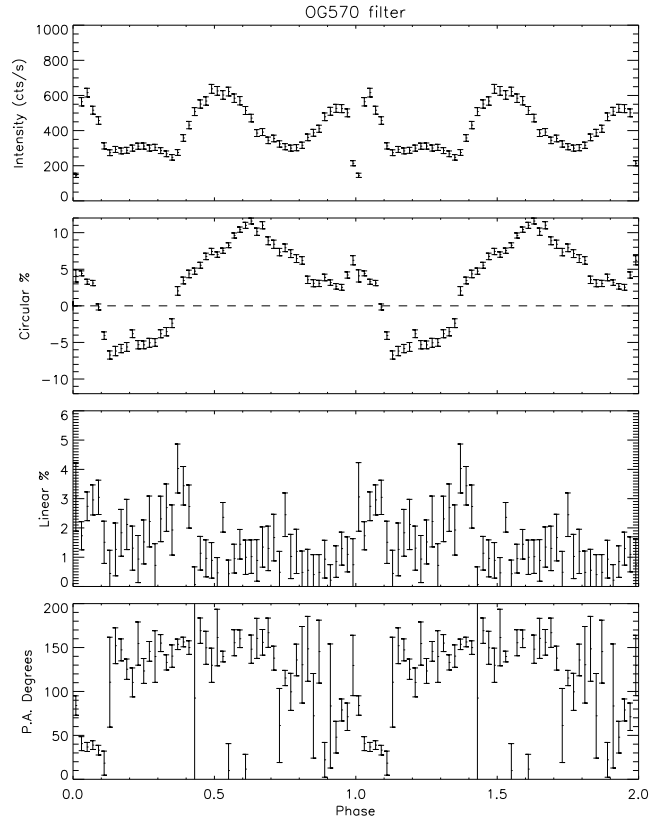


Figure 3. The polarimetric data (OG570 filter) folded on the eclipse ephemeris derived in section 3.2.

solved ingresses and egresses, the uncertainty in these measurements was taken to be the time resolution in the data. Mid-eclipse times were then calculated as the average of the the ingress and egress for a given eclipse. The times of mid-eclipses with their uncertainties are shown in (table 2).

We used the mid-point between the extremely sharp (~ 3 seconds) ingresses and egresses of the 2003 eclipses to calculate the times of mid-eclipse (see table 2). A least squares polynomial fit (order 1) gives an orbital period of 0.0701623d with an error of $5.7 \times 10^{-7}\text{d}$. The six year gap between the 1996 and the 2003 observations correspond to ~ 37000 orbital cycles, giving an accumulated error of ~ 30 minutes. This is sufficiently small to assign unambiguously cycle counts to the 1996 eclipses, as well as to those observed in 2003. A least squares polynomial fit (order 1) to the times

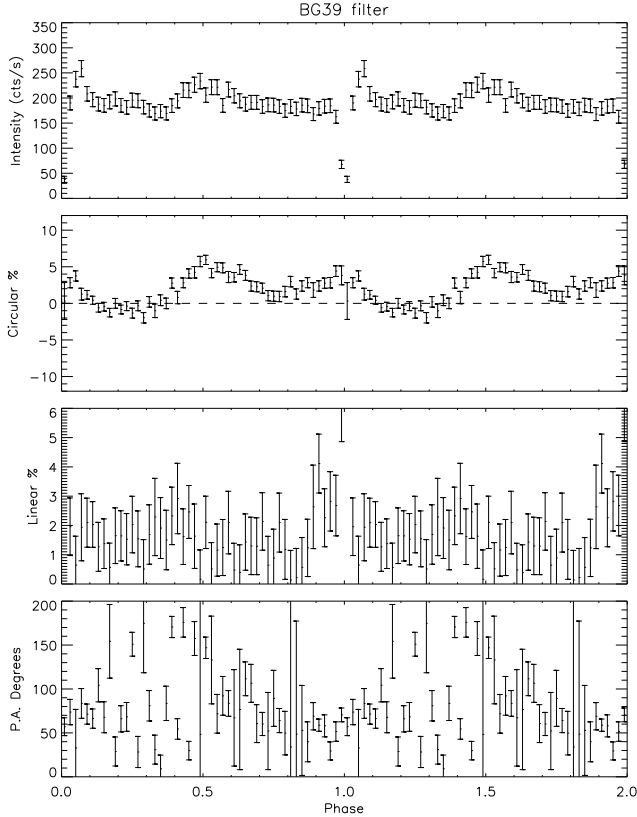


Figure 4. The polarimetric data (BG39 filter) folded on the eclipse ephemeris derived in section 3.2.

of mid-eclipse of both datasets together yields the following eclipse ephemeris:

$$T(HJD) = 2452879.2813386(58) + 0.070162312(9)E$$

From the 2003 eclipses alone, we calculate the average of the total eclipse time to be 177 ± 2.3 seconds, which corresponds to $\Delta\phi = 0.0292 \pm 0.0004$ of the orbit. The error is estimated from the standard deviation.

3.3 The photometry

Phase-folded photometric light-curves are presented in Figs. 2, 3 & 4.

As can be seen from these figures, there is a bright phase occurring just before the eclipse. In contrast, the bright phase is more centered on the eclipse during the low state 1996 observations (see Tappert, Augusteijn & Maza 2004). A similar effect has been seen in other eclipsing polars, e.g. HU Aqr (Schwope et al. 2001), and can be explained as the relocation of an accretion region on the surface of the white dwarf between high and low states. During the low state, the ballistic stream is thought to attach to magnetic field lines soon after leaving the inner Lagrangian point. Consequently, the accretion region forms relatively close to the line of centers of the two stars, causing the bright phase to be centered approximately on the eclipse. During the high state, however, the ballistic stream has more ram pressure,

so it is able to penetrate further around the white dwarf before attaching to magnetic field lines. As a result, the accretion region is located further in longitude from the line of centers of the two stars, and the center of the bright phase then occurs sometime before the eclipse.

The double-humped nature of the bright phase is discussed in the next section.

3.4 The polarimetry

Figs. 2, 3 & 4 also show the unfiltered, OG570 & BG39 polarimetric observations, respectively, folded and binned on the orbital ephemeris derived in section 3.2. As can be seen from these figures, the polarimetry shows both positive and negative circular polarization. This is typical of accretion onto two regions on the surface of the white dwarf which are located close to magnetic poles of opposite magnetic polarity (e.g. Buckley & Shafter 1995).

The bright phase in the photometry and polarimetry show the typical morphological features of cyclotron emission from a magnetically confined accretion shock on the surface of the white dwarf, namely a double-humped variation due to the angular dependence of the beaming of the cyclotron radiation, and a wavelength dependence. Most of the polarized flux is seen through the red (OG570) filter, with the circular polarization rising to 12 percent. Polarized flux rises to a maximum of 5 percent through the blue (BG39) filter. This is typical of polars with magnetic field strengths of about ~ 20 MG (e.g. ST LMi: Peacock et al. 1992). This magnetic field strength is consistent with the Zeeman splitting of the white dwarf absorption lines reported in Tappert, Augusteijn & Maza 2004.

The bright phase lasts ~ 0.75 of an orbit, indicating that the main accretion region is located in the hemisphere closest to Earth (say, the upper hemisphere). As a rough starting point for Stokes Imaging, we have used this value to estimate the magnetic dipole offset angle (β) as a function of inclination using equation 1 of Visvanathan & Wickramasinghe (1981). This equation assumes that the accretion region is not extended and that it is located at the magnetic pole. We argue that this is a good starting point, however, because one would expect to see a more pronounced asymmetry in the circularly polarised light curves and in the linearly polarized pulses if the accretion region was significantly extended or offset from the magnetic pole (see the cyclotron emission models of Potter 1998 and Ferrario et al. 1990, and see Bailey et al. 1995 and Ramsay et al. 1996 for examples of systems where the accretion region is thought to have a large offset from the magnetic pole). The range of inclinations is estimated using the observed eclipses and is discussed in section 3.5. The results are shown in table 3.

During the faint phase, negative circular polarization is seen in the unfiltered and red (OG570) filter only (Figs. 2, 3 and, conversely, Fig. 4), rising to a maximum of \sim (minus) 7 percent. The faint phase in the photometry and polarimetry lasts ~ 0.25 of an orbit, indicating that the second accretion region is located in the hemisphere of the white dwarf farthest from Earth (the lower hemisphere). Although it is possible that the lower accretion region is in view for a longer period than that indicated by the negative circular polarization, there is no evidence of this in our data (e.g. linear pulses at phases different from those described below).

There are two linearly polarized pulses centered on phases ~ 0.4 and ~ 0.05 , most evident in the unfiltered and OG570 observations (Figs. 2 & 3). These coincide with the reversals in the circular polarization and thus mark the appearance/disappearance of one or both accreting regions over the limb of the white dwarf, at which time the accreting field lines are viewed perpendicularly from Earth. The variation in position angle is poorly defined for most of the orbit, except at the phases of the linearly polarized pulses.

3.5 The system's geometry and dimensions

We now use the eclipses and the system's parameters derived so far in order to investigate the system's geometry and dimensions.

The mass and radius of the secondary star can be estimated by using the mean empirical mass-period and radius-period relationships (Smith & Dhillon 1998) i.e.

$$M2/M_{\odot} = (0.126 \pm 0.011)P - (0.11 \pm 0.04) = 0.1(\pm 0.06)$$

and

$$R2/R_{\odot} = (0.117 \pm 0.004)P - (0.041 \pm 0.018) = 0.16(\pm 0.03)$$

Next, we use the fact that the duration of the total eclipse of the primary is a function of the mass-ratio and the inclination only. This cannot be expressed in an analytical form. However, Horne (1985) presented a graphical representation of this relationship as a function of eclipse width, which we now use to investigate the mass ratio-inclination parameter space.

For stable mass transfer we require that $M2/M1 < 1$ and, therefore, using the above estimate of $M2 = 0.1M_{\odot}$, the mass of the white dwarf primary must be $0.1 < M1 < 1.44M_{\odot}$, which is equivalent to $0.069 < M2/M1 < 1$. Using this and the eclipse length of $\Delta\phi = 0.029$ (derived from section 3.2) in conjunction with figure 2 of Horne (1985), we find that the inclination must be in the range $70^{\circ} < i < 81.5^{\circ}$. Propagating the errors for the mass of the secondary increases the upper limit to 85° . We also estimate a range for the white dwarf radius (see Hamada & Salpeter 1961 or In-Saeng Suh & Mathews 2000). These parameters are tabulated in table 3 as a function of inclination.

3.6 Modelling the cyclotron emission.

We next model the polarization data using the Stokes imaging technique of Potter, Hakala & Cropper (1998) and Potter et al. (2004). Stokes imaging allows the mapping of the accretion region(s) (strictly speaking, the cyclotron emission regions) in magnetic cataclysmic variables in terms of their location, shape and size. Any particular solution depends on certain system's parameters (inclination and the dipole offset angles in latitude and longitude), so the technique was run several times in order to investigate the solutions within the parameter space defined by the range in our derived system's parameters.

The ranges in the binary inclination and the β offset of the magnetic pole were estimated in the previous sections and tabulated in table 3. We now estimate the longitude of the magnetic pole (how far ahead it is from the line of

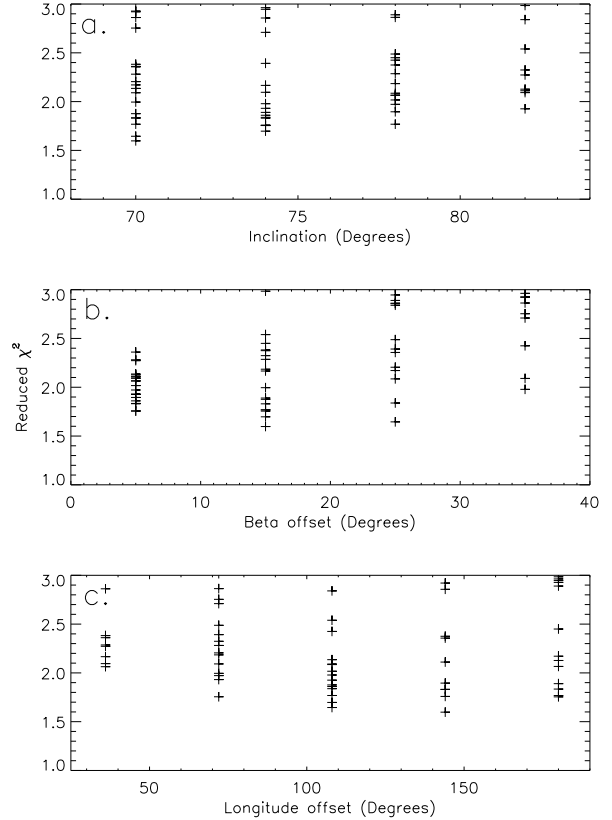


Figure 5. Final reduced χ^2 from running Stokes imaging several times, each assuming different values of the inclination and magnetic dipole offset angles. Results plotted as a function of a) inclination b) the magnetic dipole offset (β) and c) the magnetic dipole offset in longitude.

centers of the two stars) by assuming that the upper accretion region is located close to the magnetic pole. Then, from Figs. 2,3 & 4, it can be seen that the upper accretion region is eclipsed by the secondary star towards the end of the bright phase. This is ~ 0.3 of an orbit after the upper accretion region is most face on to the viewer. This indicates that the upper accretion region, and hence the upper magnetic pole, is ahead ($\sim 100^{\circ}$ in longitude) of the line of centers of the two stars.

Figs. 5 a,b & c show the final reduced χ^2 from running Stokes imaging several times, each assuming different values of the inclination and magnetic dipole offset angles. The technique of Potter, Hakala & Cropper (1998) included an estimate of the smoothness of the predicted emission region in the final fit. However, we use the methodology outlined in Potter et al. (2004) in which emission regions are smooth from the outset and therefore the final reduced χ^2 does not contain any extra terms. The three plots refer to the same set of solutions, each plotted as a function of a different parameter. The final reduced χ^2 of the model fit to the observations for a particular set of system parameters is represented by a '+''. For each value of one of the parameters, there is a range in χ^2 corresponding to the fits for different combinations of the other parameters. Hence, each solution appears once in every plot.

Formally, the best solution is obtained using an inclina-

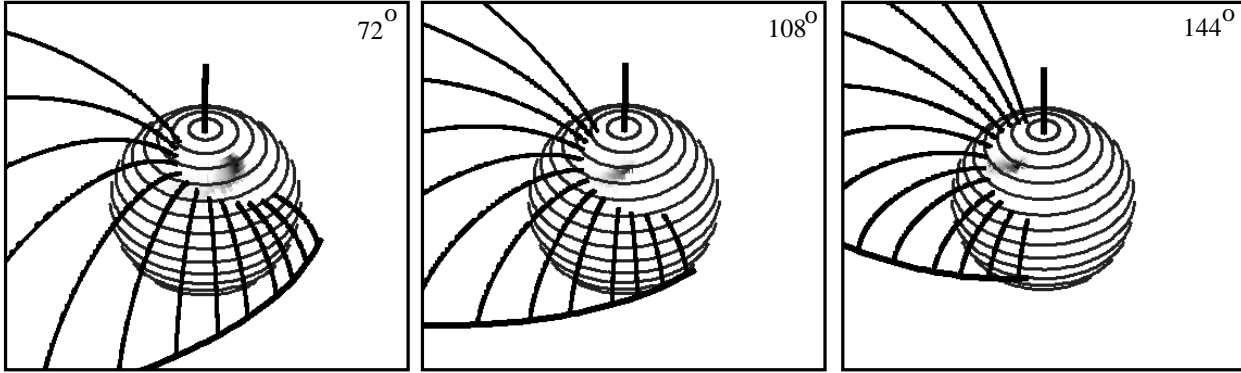


Figure 6. Predictions for the shape, size and location of the upper accretion region (grey shaded area) assuming a binary inclination of 70° , magnetic dipole offset $\beta = 5^\circ$ and magnetic dipole longitude of 72° , 108° and 144° (from left to right). The globes represent the surface of the white dwarf with latitudes marked every 10 degrees. The upper magnetic pole is indicated by a vertical straight line. The remaining solid curves represent magnetic field lines. The white dwarf rotates in a anti-clockwise direction as seen from above the upper spin axis. The white dwarf is orientated such that the upper magnetic pole is most parallel to the viewers line of sight.

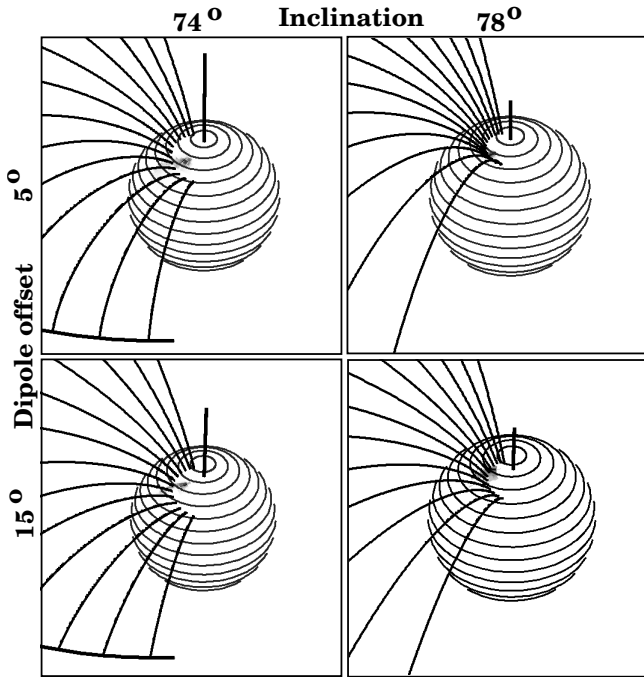


Figure 7. As in Fig. 6 except, from left to right, binary inclinations of 74° and 78° , and, from top to bottom, magnetic dipole offset angles of $\beta = 5^\circ$ and $\beta = 15^\circ$. A magnetic dipole longitude of 144° was assumed in all cases.

tion of 70° and dipole offset angles of 15° and 144° for latitude and longitude, respectively. However, given the shallowness of the minima in Fig. 5, we next investigate the actual shape, size and location of the accretion regions on the surface of the white dwarf predicted by Stokes imaging.

3.6.1 The upper accretion region.

We first concentrate on the solutions for the emission from the upper accretion region only (the bright phase) because the polarized emission from the upper accretion region is visible for a larger fraction of the orbit than the lower accretion region. The visibility of the upper accretion region

is clearly demarcated by the positive circular polarization and by the beginning and end points of the bright phase in the photometry. Therefore, there is no ambiguity associated with the visibility of the upper accretion region.

We now investigate the solutions with different values for the longitudinal offset of the magnetic dipole. Fig. 6 shows three solutions from Stokes imaging. From left to right, the magnetic longitude was set to be 72° , 108° and 144° . Each solution assumed an inclination of 70° and a magnetic dipole offset angle of $\beta = 5^\circ$. The accretion region is shown as the shaded grey area.

In each case we have overplotted a model ballistic trajectory computed using a single particle under gravitational and rotational influences only. No additional drag terms (e.g. due to the magnetic field) are included. The particle is allowed to follow a ballistic path from the L1 point and is terminated 130 degrees in azimuth around the white dwarf. At 10 degree intervals in azimuth (from 0 to 130 degrees) around the white dwarf, dipole trajectories are calculated (the curved diagonal lines) from the ballistic stream to the surface of the white dwarf. The mass ratio and white dwarf mass were assumed to be as given in table 3. For a particular white dwarf mass and inclination, the smaller white dwarf radius of the range defined in table 3 was assumed.

We next compare the location of the footprints of the magnetic field lines on the surface of the white dwarf with the prediction for the location of the upper accretion region. This comparison serves to check the validity of the predictions from Stokes imaging: the two locations should be very similar.

The left and middle solutions of fig. 6 are rejected for two reasons. Firstly, the location of the accretion region is found not to be trailing the magnetic pole in orbital phase. The asymmetry in the double-humped morphology of the bright phase in the photometry and, in particular, in the positive circular polarisation suggests that the accretion region trails the magnetic pole (see the discussion in section 3.4 and Cropper 1998 for an example of where the accretion region is thought to be ahead of the magnetic pole). Therefore, we reject any of the solutions that predicted the upper accretion region to be ahead of the upper magnetic

pole. Secondly, because the footprints of the magnetic field lines do not overlap with the accretion region.

The right plot, however, shows the location of the accretion region to be trailing the magnetic pole. The overlap between the magnetic footprints and the accretion region is slightly better, but could not be improved by increasing the longitude of the magnetic pole. In addition, for angles larger than 180° , the χ^2 fit becomes increasingly worse. We would like to point out that we have used the smallest white dwarf radius possible as defined by the white dwarf mass radius relationship (see Hamada & Salpeter 1961 or In-Saeng Suh & Mathews 2000) and permitted by the estimate of the system's parameters of table 3. Increasing the white dwarf radius decreases the overlap.

Thus we can conclude that magnetic dipole longitudes smaller than $\sim 144^\circ$ are inconsistent with the modelling of the polarimetry and incorrectly predict the accretion region to lead the magnetic pole in orbital phase. This conclusion was reached by assuming that accretion takes place from the unperturbed ballistic stream threaded by unperturbed magnetic field lines, which is clearly too simplistic. However, we argue that a more detailed model that includes additional effects, such as magnetic drag, would give rise to a stream that has smaller orbital velocities and would, most probably, place it on a trajectory on the inside of the unperturbed ballistic trajectory (see Heerlein, Horne & Schwope 1999 for an investigation into the effects of additional drag terms). Consequently, once attached to the magnetic field lines, the footprints would be located even further to the left of the accretion regions compared to those shown in Fig. 6.

Therefore, in what follows, the magnetic longitude is fixed at $\sim 144^\circ$ and we investigate the solutions for different inclinations and β offsets.

We now examine the solutions as a function of inclination. For inclinations less than 74 degrees, the magnetic footprints were found to be always at lower latitudes than the accretion region predicted by Stokes imaging, as already demonstrated in Fig. 6. For inclinations of $\sim 74^\circ$ the overlap was marginal, and it's best for inclinations of $\sim 78^\circ$ (Fig. 7). This is towards the middle of the range in inclination estimated from using the eclipse length in combination with figure 2 of Horne (1985) (see section 3.5 above). Inclinations of $\sim 78^\circ$ are also more in agreement with the implied mass ratios and primary masses (table 3) expected for CVs with similar orbital periods (Smith & Dhillon 1998). We have assumed that the difference in primary masses between magnetic and nonmagnetic white dwarfs to be insignificant assuming the magnetic field strength used here (see In-Saeng Suh & Mathews 2000).

Fig. 7 also shows the solutions for different values for the β offset of the magnetic dipole. Good overlap between the magnetic footprints and the predicted location of the upper accretion region from Stokes imaging is found for β angles of 5 and 15° . The reduced χ^2 fit, as a function of β offset angle (Fig. 5 b), also predicts best values within this range.

3.6.2 The lower accretion region.

As described earlier, it is more difficult to be certain of the phases at which this accretion region is in view. However, we can assume that the lower accretion region is in view

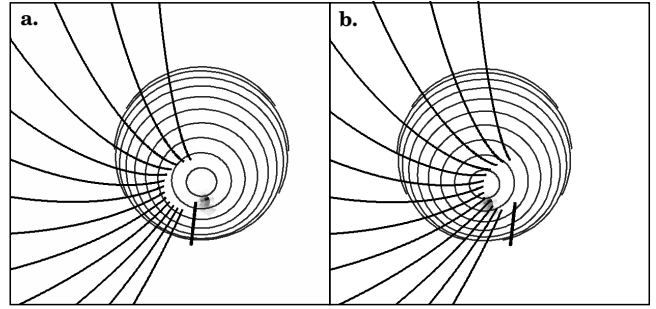


Figure 8. a. Predictions for the shape, size and location of the lower accretion region viewed from above the lower spin axis of the white dwarf. b. As a) except the lower magnetic pole has been moved in order to ‘force’ the magnetic field lines to overlap with the lower accretion region (see text)

for a phase range at least defined by the appearance of the negative circular polarization.

The same values for the inclination, mass-ratio and white dwarf mass that gave the best results for the upper accretion region were used. However, we found that by using the same dipole geometry for the upper accretion region, the lower footprints of the magnetic fieldlines, from the same ballistic stream, did not coincide with the lower accretion region predicted by Stokes imaging (Fig. 8 a). Not surprisingly, this can be accounted for by assuming that the magnetic field of the white dwarf is not simply a tilted dipole. Fig. 8 b. shows that by offsetting the lower magnetic pole in longitude and latitude by $\sim 30^\circ$ and $\sim 10^\circ$ respectively, whilst keeping the upper magnetic pole fixed, the magnetic footprints can be ‘forced’ to coincide with the lower accretion region. However, it should be noted that, as mentioned above, the location of the lower accretion region may be incorrect due to the possible lack of phase coverage given by the negative polarisation.

If the magnetic field geometry were different from that of a simple dipole, it would not be possible to obtain a unique magnetic field geometry by modelling both accretion regions simultaneously. However, the polarized emission from *one* accretion region located close to a magnetic pole is only weakly dependent of the magnetic field topology of the white dwarf as a whole. This is because the inclination of the magnetic field lines close to a magnetic pole are very similar for most magnetic field topologies. Therefore, the conclusions drawn in section 3.6.1 for the upper accretion region would not be expected to require significant modification.

3.6.3 The model light curves.

The model light curves (for both accretion regions) for an inclination of 74° , magnetic dipole angles of 144° and 5° are shown overplotted on the polarimetric observations in Fig. 2. Note that the aim of Stokes imaging is to fit the general morphological variations of the observations, but not to fit the small scale details that either cannot be distinguished from noise, or that go beyond the assumptions of the cyclotron model. Hence, as can be seen from Fig. 2, the model has fit well the general variations of the light curves, namely the double-humped bright phase (intensity and circular polarization), the faint phase and the positions of the linear pulses.

The model fit is worse during phases $\sim 0.7 - 0.1$, where too much circular polarization is predicted. This may arise because the model does not take into account any additional absorption by the accretion curtain that intersects our line of sight during these phases.

4 SUMMARY AND CONCLUSIONS

We have found polarisation in the new eclipsing polar CTCV J1928-5001, thus identifying it as a polar with an orbital period of ~ 101 minutes. Our polarimetric observations show that there are two accretion regions and the white dwarf has a magnetic field strength of ~ 20 MG.

From the eclipses we estimate some of the system's parameters, which we further refine by modelling the polarimetric observations and making comparisons with calculations of single particle ballistic and magnetic trajectories.

We find the inclination to be $77^\circ \pm 2^\circ$, the offset of the upper magnetic pole from the spin axis to be between $\sim 5 - 15^\circ$ and to be no less than $\sim 144^\circ$ ahead of the line of centers of the two stars. The single particle ballistic models agree well with the results from Stokes imaging for the location of the upper accretion region within this parameter range. Agreement is not found for the location of the lower cyclotron accretion region. This could either be due to the lack of polarization from the lower accretion region, due to the dominance of emission from the upper accretion region, or to the assumption of a centered dipole being incorrect. Both reasons could also apply simultaneously. The presence of two sets of cyclotron harmonics from spectroscopic observations (e.g. Schwobe et al. 1995) could help to determine the magnetic topology (e.g. an offset dipole) of the white dwarf.

5 ACKNOWLEDGMENTS

Thanks go to E. Romero-Colmenero for valuable discussions. We would also like to thank the Referee for comments which significantly improved the paper.

REFERENCES

- Bailey Jeremy A., Ferrario Lilia, Wickramasinghe Dayal T., Buckley David A. H. & Hough, J. H., 1995, MNRAS, 272, 579
 Bridge et al., 2002, MNRAS, 336, 1129
 Buckley David A. H. & Shafter Allen W., 1995, MNRAS, 275, 61
 Cropper M. S., 1985, MNRAS, 212, 709
 Cropper Mark, 1998, MNRAS, 295, 353
 Cropper M. S., 1990, Space Sci. Rev. 54,195
 Cropper M. S., 1997, MNRAS, 289, 21
 Ferrario L. & Wickramasinghe D. T., 1990, ApJ, 357, 582
 Hakala P. J., Watson M. G., Vilhu O., Hassall B.J.M., Kellett B.J., Mason K.O. & Piirola V., 1993, MNRAS, 263, 61
 Hamada T., Salpeter, E. E., 1961, ApJ, 134, 683
 Heerlein Claus, Horne Keith & Schwobe Axel D., 1999, MNRAS, 304, 145
 Horne K., 1985, MNRAS, 213, 129
 Hsu J. C. & Breger M., 1982, ApJ, 262, 732
 Imamura James N., Steiman-Cameron, Thomas Y., 1998, ApJ, 501, 830
 Katajainen S. et al. 2003, MNRAS, 340, 1
 Peacock Tim, Cropper Mark, Bailey Jeremy, Hough J. H. & Wickramasinghe D. T., 1992, MNRAS, 259, 583
 Potter S. B., 1998, PhD thesis, Univ. London
 Potter S. B., Hakala P. J. & Cropper Mark, 1998, MNRAS, 297, 1261
 Potter Stephen B., Romero-Colmenero E., Watson C. A., Buckley D. A. H. & Phillips A., 2004, MNRAS, 348, 316
 Ramsay Gavin, Cropper Mark, Wu Kinwah & Potter Stephen, 1996, MNRAS, 282, 726
 Romero-Colmenero E., Potter Stephen B., Buckley D. A. H., Barrett P. E., Vrielmann S., 2003, MNRAS, 339, 685
 Schwobe A. D., Thomas H. -C., Beuermann K., Burwitz V., Jordan S. & Haefner R., 1995, A&A, 293, 764
 Schwobe Axel D., Cataln Maria S., Beuermann Klaus, Metzner Andr, Smith Robert Cannon, Steeghs Danny, 2000, MNRAS, 313, 533
 Schwobe A. D., Schwarz R., Sirk M., Howell S. B., 2001, A&A, 375, 419
 Smith D. A. & Dhillon V. S., 1998, MNRAS, 301, 767
 Suh In-Saeng, Mathews G. J., 2000, ApJ, 530, 949
 Tappert C., Augusteijn T. & Maza J., 2004, MNRAS, 354, 321
 Visvanathan N. & Wickramasinghe D. T., 1981, MNRAS, 196, 275
 Warner B. 1995, Cataclysmic Variable Stars, Cambridge Astrophysics Series 28, Cambridge University Press